Journal of Molecular Spectroscopy 323 (2016) 53–58

Contents lists available at ScienceDirect

Journal of Molecular Spectroscopy

journal homepage: www.elsevier.com/locate/jms

Temperature-dependent absorption cross-sections of perfluorotributylamine

Paul J. Godin [a,*], Alex Cabaj [a], Stephanie Conway [a], Angela C. Hong [b], Karine Le Bris [c], Scott A. Mabury [b], Kimberly Strong [a]

[a] Department of Physics, University of Toronto, 60 St. George St., Toronto, ON M5S 1A7, Canada
[b] Department of Chemistry, University of Toronto, 80 St. George St., Toronto, ON M5S 3H6, Canada
[c] Department of Physics, St. Francis Xavier University, Antigonish, Nova Scotia B2G 2W5, Canada

ARTICLE INFO

Article history:
Received 1 October 2015
In revised form 20 November 2015
Accepted 24 November 2015
Available online 2 December 2015

Keywords:
Perfluorotributylamine
FTIR
Radiative efficiency
Global warming potential
Absorption cross-section
Density functional theory

ABSTRACT

Cross-sections of perfluorotributylamine (PFTBA) were derived from Fourier transform spectroscopy at 570–3400 cm^{-1} with a resolution of 0.1 cm^{-1} over a temperature range of 298–344 K. These results were compared to theoretical density functional theory (DFT) calculations and to previous measurements of PFTBA made at room temperature. DFT calculations were performed using the B3LYP method and the 6-311G(d,p) basis set.

We find good agreement between our experimentally derived results, DFT calculations, and previously published data. No significant temperature dependence in the PFTBA cross-sections was observed for the temperature range studied. We calculate an average integrated band strength of 7.81×10^{-16} cm/molecule for PFTBA over the spectral range studied. Radiative efficiencies (RE) and global warming potentials (GWP) for PFTBA were also derived. The calculated radiative efficiencies show no dependence on temperature and agree with prior publications. We find an average RE of 0.77 Wm^{-2} $ppbv^{-1}$ and a range of GWP from 6874 to 7571 depending on the lifetime used. Our findings are consistent with previous studies and increase our confidence in the value of the GWP of PFTBA.

1. Introduction

Perfluorotributylamine (PFTBA) is a fully-fluorinated liquid ($N(CF_2CF_2CF_2CF_3)_3$ as shown in Fig. 1) commonly used in electronic reliability and quality testing, and heat transfer applications. PFTBA belongs to the class of perfluoroalkyl amines, which are chemically stable liquids with no known sinks in the atmosphere, resulting in lifetimes of hundreds of years and well-mixed atmospheric distributions. Furthermore, as compounds containing C–F bonds, they absorb strongly in the optically thin region of the atmosphere known as the atmospheric window (750–1250 cm^{-1}), which, in turn, results in positive radiative forcing. Due to this, PFTBA is considered a potential long-lived greenhouse gas (LLGHG).

Global warming potential (GWP) is a useful metric to determine the radiative impact of a chemical on the atmosphere. A GWP measures the radiative forcing (RF) of a unit mass of a trace gas compared to an equal mass of carbon dioxide, while taking into account the lifetime of the species in the atmosphere. Despite their low mixing ratios, halocarbons contribute a significant amount to radiative forcing in the atmosphere [1]. The RF of a trace gas can be calculated from its radiative efficiency (RE), which in turn can be calculated from its absorption cross-section. A recent paper by Hong et al. determined that PFTBA has the largest RE of any compound detected in the atmosphere [2], having a volume mixing ratio (VMR) of 0.18 ± 0.01 pptv and a RE of 0.86 Wm^{-2} $ppbv^{-1}$. Furthermore, there are currently no policies in place which require industry to report production or emission values for PFTBA, resulting in high uncertainty of its VMR trend and climate impacts.

Currently, the only published spectrum of PFTBA was recorded at 296 K at 1.54–4.26 mTorr in a 760 Torr N_2 background at a resolution of 0.25 cm^{-1} using 32 co-added spectra [2]. In this work, we present the first known temperature-dependent measurements of PFTBA; these measurements are compared to theoretical density functional theory (DFT) calculations and the previously published data. Additionally, we calculate the RE and GWP for PFTBA.

2. Experimental setup

The absorption spectra were obtained using a Bomem DA8.002 Fourier transform spectrometer with a globar source and a KBr beamsplitter. Spectra were recorded from 570 to 1400 cm^{-1} at a

* Corresponding author.
E-mail address: pgodin@physics.utoronto.ca (P.J. Godin).

http://dx.doi.org/10.1016/j.jms.2015.11.004
0022-2852/

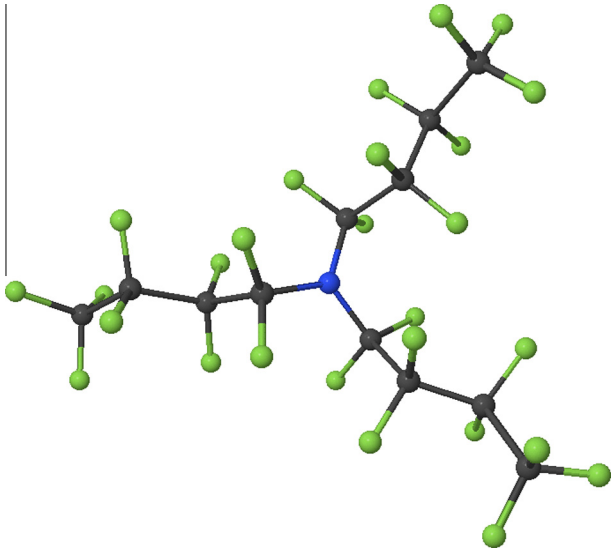

Fig. 1. Projection image of PFTBA. The blue atom is nitrogen, the green atoms are fluorine, and the grey atoms are carbon.

resolution of 0.1 cm^{-1}. These parameters were chosen as no fine-scale spectral features were seen at higher resolution and no features were observed outside of this range (down to 300 cm^{-1} and up to 3400 cm^{-1}). Each measurement consists of 500 co-added spectra.

The gas sample was allowed to diffuse into a 10.0 ± 0.1 cm long stainless-steel heatable cell in order to reach the desired pressures. Temperature control was provided by electric heating bands attached to a voltage control. The temperature was measured by an in-line thermocouple inside the cell. Wedged ZnSe windows with Buna-N o-rings were used to seal the ends of the cell. The infrared beam was measured using a liquid-nitrogen-cooled mercury cadmium telluride (MCT) detector.

The PFTBA sample was a commercial product from Sigma–Aldrich (certified $99 \pm 0.5\%$ pure). Before allowing the sample into the cell, it was subject to multiple freeze–pump–thaw cycles to remove any contaminant trace gases from the sample flask. The cell was evacuated using a Varion 250 turbo pump. The pressure was measured using a 10 Torr MKS baratron pressure gauge. The cell's leak rate is approximately 0.03 Torr/h. Over a two-hour-long measurement, this added pressure does not significantly alter the spectrum.

PFTBA has a low vapour pressure, limiting the range of accessible pressures for a given temperature. Vapour pressures are calculated using the August Equation, which relates pressure and temperature using chemical specific constants A and B:

$$\log(P) = A - \frac{B}{T}. \tag{1}$$

For PFTBA, $A = 10.511$ and $B = 2453$ K [3]. This results in low vapour pressures at temperatures below 298 K. In order to access a larger pressure range to achieve good signal-to-noise ratios, we chose to study temperatures in the range of 298–344 K. At each temperature, measurements were made at 7–10 different pressures in the range of 0.1–1.1 Torr.

Heating of the input aperture produces a second blackbody source; by adding a second (exit) aperture after the interferometer, this second source is removed [4]. Both apertures in the system were set to 3.5 mm diameter, which allows for a resolution of 0.1 cm^{-1} [5]. Fluctuations in the lab temperature and ambient air can also affect the measurements. To minimize these effects, the cell is enclosed in a vacuum jacket to isolate it from the environment; this second chamber achieves pressures under 3.0 Torr. Empty cell scans are performed in between filled cell runs to monitor baseline stability. Locations of known zero absorption are adjusted in the filled cell scan to match the baseline in order to remove any fluctuations in globar intensity.

3. Data analysis

The absorption of light by a medium at a given pressure and temperature (P, T) can be described by the well-known Beer–Lambert Law:

$$I(\nu) = I_o(\nu)e^{-\chi(\nu)} \tag{2}$$

where $I(\nu)$ is the intensity after passing through the gas sample, $I_o(\nu)$ is the incident (baseline) intensity, and $\chi(\nu)$ is the optical depth given by:

$$\chi(\nu) = \frac{PT_o}{TP_o} N_L L \sigma(\nu) \tag{3}$$

where P_o and T_o are standard conditions for pressure and temperature, N_L is Loschmidt's constant, L is the cell length, and $\sigma(\nu)$ is the apparent absorption cross-section. The apparent cross-section varies linearly with pressure as [11]:

$$\sigma(\nu) = A(\nu)P + \sigma_{real}(\nu) \tag{4}$$

where $A(\nu)$ is a fitting coefficient and $\sigma_{real}(\nu)$ is the absorption cross-section at the zero-pressure limit. Inserting Eq. (4) into Eq. (3) yields:

$$\chi(\nu) = \frac{PT_o}{TP_o} N_L L[A(\nu)P + \sigma_{real}(\nu)]. \tag{5}$$

Now the real cross-section can be found via a fit of optical depth to pressure for a given temperature and wavenumber. All fits have a forced convergence of $\chi = 0$ for $P = 0$.

Large molecules with high molecular weights have large moments of inertia, resulting in many rotational-vibrational transitions. Inherently, it is difficult to obtain precise lineshapes for heavy molecules, as their infrared absorption spectra characteristically possesses broad bands arising from the overlap of multiple individual spectral transitions, combination bands, and hot bands making it difficult to resolve line-by-line transitions. For PFTBA, there is so much overlap that we are unable to even distinguish PQR branches. In this case, instead of attempting to extract line parameters, it is more convenient to integrate the absorption cross-section and report the integrated band strengths for a defined wavenumber region:

$$S = \int \sigma_{real}(\nu) d\nu. \tag{6}$$

Previous publications using the same set-up describe our error analysis, which we summarize here [6–10]. Following those papers, sources of error include temperature fluctuations (±0.2 K), pressure readout (±0.015 Torr), path length (±1 mm), and sample purity (±0.5%). These errors are propagated in the calculation of the apparent cross-section to get its uncertainty. The uncertainty of the apparent cross-section is used to assign weights in the fit to find the real cross-section. The remaining sources of error due to the non-linearity of the MCT detector, baseline drift, data reduction, and instrument noise can be accounted for in the fit to optical depth, which is chosen at the 95% confidence limit. Only points with an optical depth between 0 and 1.1 are processed. This selection avoids non-physical (negative absorption) and non-linear detector effects. The final reported uncertainty is the 95% confidence limit of the quadratic fit.

4. Results and data validation

Measured absorption cross-sections as a function of temperature are shown in Fig. 2. The vertical black lines indicate the regions used to calculate the integrated absorption band strengths: 570–675, 675–770, 770–900, 900–1025, and 1025–1400 cm^{-1}. The integrated band strengths as a function of temperature are shown in Fig. 3. Total integrated band strength show no significant change with temperature. While the population of individual bands could change with temperature, due to the population of one band increasing as the result of a decrease in another band, this effect is not observed.

Integrated bands strengths are reported in Table 1. Within our error bars, we see good agreement with previously published data [2]. It should be noted that the initial purity of the sample used in the previously published data is unknown. Furthermore, when calculating the integrated band intensities we noticed a discrepancy between their published value for total integrated band strength and what we calculated from their raw data file; instead of a value of 7.08×10^{-16} cm/molecule, we found a value of 8.47×10^{-16} cm/molecule. For consistency in this work, we use the values of integrated band strength that we calculated from the supplementary data files in [2].

Additionally, the centroid of each band as a function of temperature is shown in Fig. 4. The centroid is defined as the centre of the band weighted by intensity of the cross-sections in the band. A shift in the position of the centroid would suggest the presence of new hot bands. We see no significant trend in the position of the centroid as a function of temperature for any of the bands, supporting our claim that temperature has no significant impact on PFTBA in the range studied.

Theoretical DFT calculations were performed using *Gaussian* 03 [12] to predict the optimal molecular geometry and harmonic frequencies corresponding to the vibrational modes of PFTBA. The DFT spectrum was optimized by starting at low levels of accuracy and gradually increasing the complexity of the basis sets after each run. The final ground state geometries and vibrational frequencies of PFTBA were determined using the 6-311G(d,p) basis set and B3LYP functionals at standard pressure and temperature with a resolution of 0.679 cm^{-1}. Higher levels of theory failed to converge. The result of these theoretical calculations is shown in Fig. 2. As this calculation is for the ground state, other spectral features, such as hot bands, can be present in the experimental spectra but not in the DFT result.

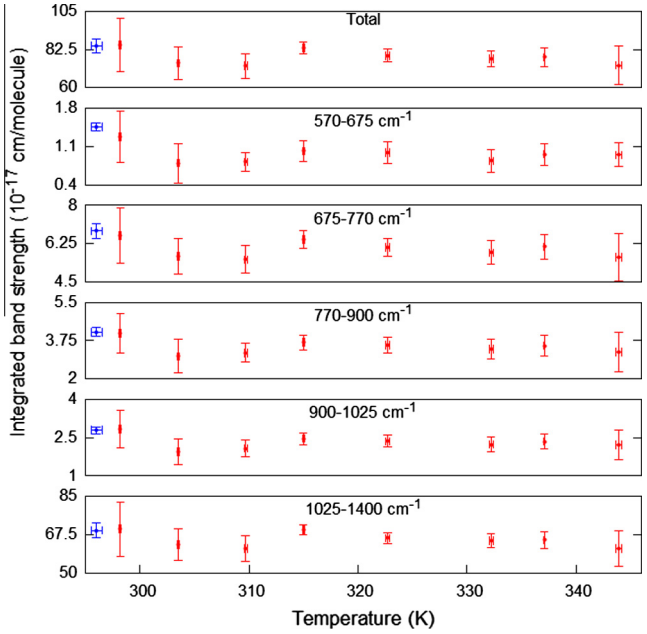

Fig. 3. Integrated band strengths for PFTBA at different temperatures. Red points are from this work and the blue points are the previously published data from [2] calculated using our method. The error in temperature is the standard deviation from all measurements taken at that temperature. The error in integrated band strength is the integrated error of the cross-section. (For interpretation of the references to colour in this figure legend, the reader is referred to the web version of this article.)

We express the integrated band strengths of each band as a fraction of the total integrated band strength, as shown in Fig. 5. We compare our DFT calculations only to the 298.2 K measurement and to Hong et al. [2], as these are the lowest temperatures, thus most likely to match with the ground state spectrum predicted by DFT. We see excellent agreement between theory and experimental results for the fractional strength of each band.

Furthermore, we identify peaks in the experimental and theoretical spectra, to evaluate how well the theory determines

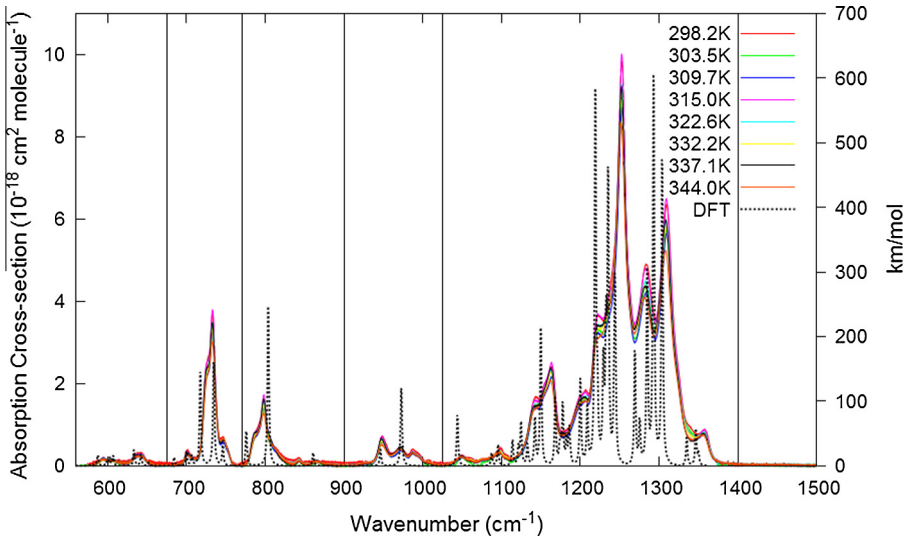

Fig. 2. Comparison of experimental cross-section of PFTBA with DFT calculation. Experimental axis is in units of cm^2/molecule, while DFT is in units of km/mol. The absorption bands are identified by the vertical black lines. Bands are defined from 570 to 675, 675 to 770, 770 to 900, 900 to 1025, and 1025 to 1400 cm^{-1}.

Table 1
Integrated band strengths of PFTBA at different temperatures.

Temperature (K)	Integrated band strengths (10^{-17} cm/molecule)					
	Total	570–675 cm^{-1}	675–770 cm^{-1}	770–900 cm^{-1}	900–1025 cm^{-1}	1025–1400 cm^{-1}
296.0 ± 0.5[2][a]	84.67 ± 4.23	1.460 ± 0.073	6.824 ± 0.341	4.142 ± 0.207	2.793 ± 0.140	69.45 ± 3.47
298.2 ± 0.11	85.05 ± 15.8	1.282 ± 0.476	6.623 ± 1.252	4.095 ± 0.910	2.845 ± 0.742	70.20 ± 12.5
303.5 ± 0.08	74.53 ± 9.63	0.796 ± 0.362	5.669 ± 0.820	3.030 ± 0.765	1.947 ± 0.486	63.09 ± 7.20
309.7 ± 0.11	72.85 ± 7.27	0.819 ± 0.168	5.521 ± 0.638	3.187 ± 0.433	2.080 ± 0.319	61.24 ± 5.71
315.0 ± 0.11	83.37 ± 3.60	1.019 ± 0.192	6.432 ± 0.396	3.669 ± 0.348	2.465 ± 0.227	69.78 ± 2.44
322.7 ± 0.18	78.90 ± 3.88	0.988 ± 0.202	6.079 ± 0.425	3.536 ± 0.362	2.358 ± 0.229	65.94 ± 2.66
332.2 ± 0.18	77.14 ± 4.79	0.837 ± 0.210	5.834 ± 0.538	3.366 ± 0.435	2.234 ± 0.294	64.87 ± 3.31
337.1 ± 0.06	77.96 ± 5.43	0.960 ± 0.201	6.103 ± 0.565	3.519 ± 0.466	2.346 ± 0.284	65.03 ± 3.91
344.0 ± 0.28	73.16 ± 11.1	0.946 ± 0.218	5.615 ± 1.096	3.229 ± 0.919	2.209 ± 0.587	61.16 ± 8.32

[a] Calculated in this work using cross-section from [2].

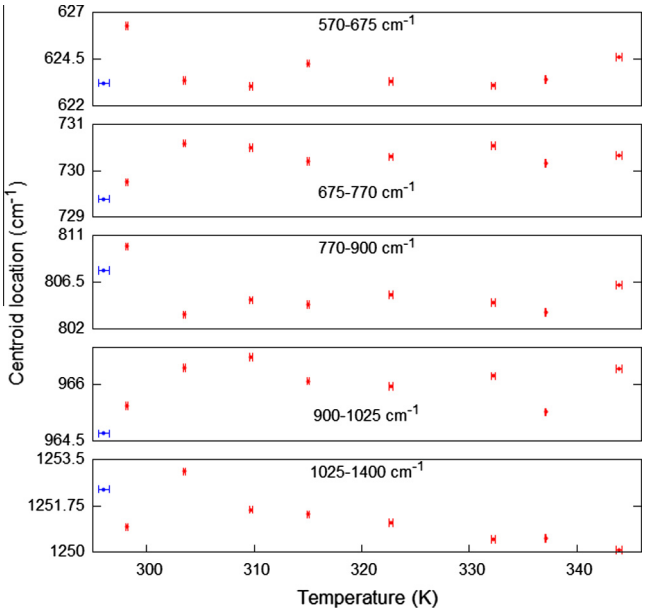

Fig. 4. Position of the centroid in each band of PFTBA at different temperatures. Red points are from this work and the blue points are the previously published data from [2] calculated using our method. The error in temperature is the standard deviation from all measurements taken at that temperature. (For interpretation of the references to colour in this figure legend, the reader is referred to the web version of this article.)

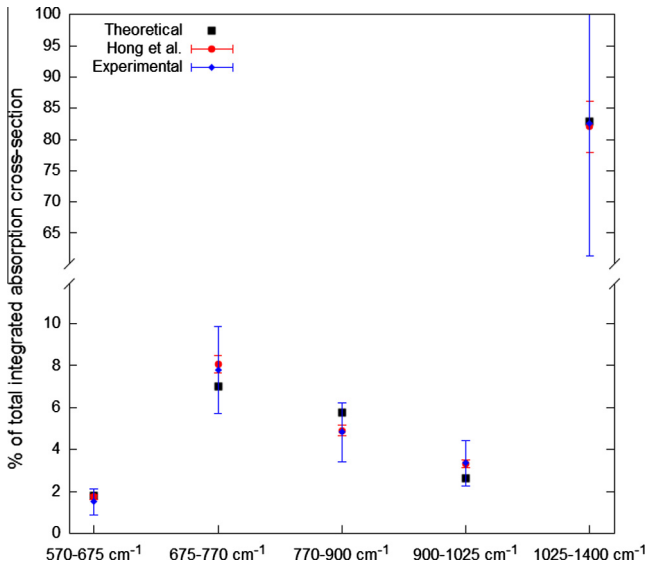

Fig. 5. Fraction of total integrated band strength due to each band. Uncertainties are from error propagation of the uncertainty in integrated band strengths. The experimental data are at a temperature of 298.2 K and the data from [2] are at 296 K. The DFT calculation is for ground state transitions only.

the position of each transition.The experimental features are much broader than the DFT predictions, often resulting in one peak in the experimental spectrum encompassing multiple DFT transitions. For such cases, the DFT peak that most closely matches the location of the centre of the experimental peak is chosen to express the theoretical location of the peak. These results are shown in Fig. 6. The average difference between the theoretical transition location and observed location at 298.2 K is -2.35 ± 3.82 cm^{-1}. While the DFT calculations do show good agreement with transition location and integrated band strength, the relative intensity between individual transitions is less successful, especially in the 1025–1400 cm^{-1} band. For example, the strongest transition in the theoretical calculations is the absorption at 1292.7 cm^{-1}, but the experimental results show the strongest absorption at 1252.8 cm^{-1}.

5. Radiative efficiencies and global warming potentials

In order to calculate the RE of PFTBA, we use the method developed by Pinnock et al. [13], which allows for the calculation of REs directly from the absorption cross-sections. Pinnock's method is to multiply the cross-section by the global annual mean atmospheric

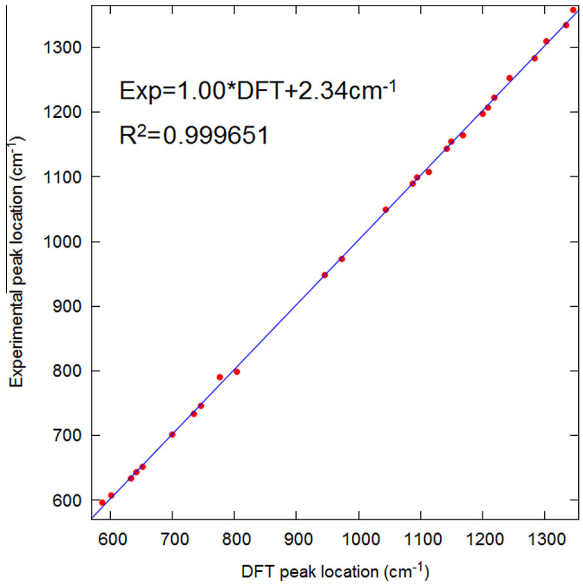

Fig. 6. DFT absorption peaks location versus experimental peak location. Fitted line has slope of 1.0 and intercept of 2.35 cm^{-1}.

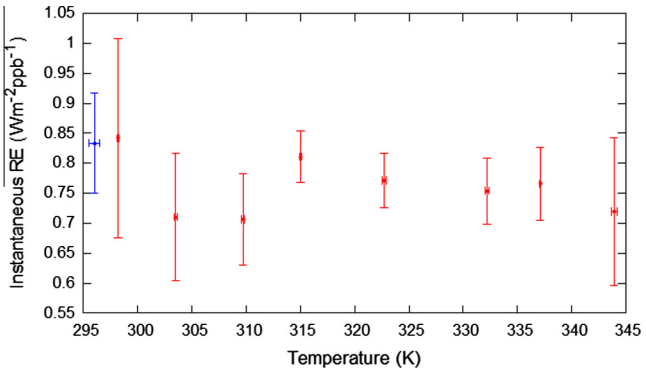

Fig. 7. Radiative efficiencies for PFTBA as a function of temperature. Red points are from this work and the blue point is the previously published data from [2] calculated using our method. The error in temperature is the standard deviation from all measurements taken at that temperature. The error in RE is the integrated error of the cross-section multiplied by the Pinnock curve. (For interpretation of the references to colour in this figure legend, the reader is referred to the web version of this article.)

instantaneous cloudy-sky RF per unit cross-section, known as a Pinnock curve, at each wavenumber. This method averages the cross-section and Pinnock curve into 10 cm^{-1} wide bins and then integrates the product over the atmospheric window range. This method achieves less than 1% error for a variety of greenhouse gases compared to more sophisticated methods.

The original Pinnock curve was calculated based on the mean atmospheric instantaneous cloudy-sky RF in 1995. Hodneborg et al. calculated an updated curve in 2012 that uses 1 cm^{-1} bins and newer atmospheric data [14]; the new Pinnock curve is calculated using the Oslo line-by-line model. We use this updated curve and condense our spectra into 1 cm^{-1} binned averages in order to calculate the RE for PFTBA at different temperatures over the range of 570–1400 cm^{-1}. The results are shown in Fig. 7. We do not observe any significant change in RE at different temperatures.

As stated earlier, a GWP is a common metric for evaluating the strength of a compound as a greenhouse gas. Explicitly, it is the time-integrated radiative forcing per unit mass over a given time horizon relative to a reference gas. The reference gas used is carbon dioxide, so for a given compound *i*, the GWP is:

$$\mathrm{GWP}(H) = \frac{\int_0^H \mathrm{RF}_i(t)\mathrm{d}t}{\int_0^H \mathrm{RF}_{\mathrm{CO_2}}(t)\mathrm{d}t} = \frac{\mathrm{AGWP}_i(H)}{\mathrm{AGWP}_{\mathrm{CO_2}}(H)} \tag{7}$$

where H is the time horizon and AGWP is the absolute global warming potential. As there are no known sinks for PFTBA, we assume an exponential decay with time in the atmosphere. From [14], this leads to an expression for the AGWP of PFTBA that depends on the radiative efficiency, lifetime (τ), and time horizon:

$$\mathrm{AGWP}_{PFTBA}(H) = \mathrm{RE}_{PFTBA}\tau\left(1 - \exp\left(-\frac{H}{\tau}\right)\right). \tag{8}$$

A time horizon of 100 years is used following common practice in international regulations.

Hodneborg et al. [14] also provide different methods to calculate GWP depending on the vertical distribution of the VMR. The Pinnock method to calculate RE assumes a well-mixed VMR. However, if the removal process is either more tropospheric (e.g., reactions with OH radicals) or stratospheric (e.g., photolysis), the shape of the VMR will not be constant. As such, corrections to the RE need to be made before calculating the GWP. Perfluorinated compounds have no known sinks in the troposphere and are usually removed by processes in the stratosphere [15,16]. However, PFTBA has a low vapour pressure at tropospheric temperatures, and would likely have a high deposition rate to the ground and thus may not be well mixed for the entire atmospheric column. Since there are no measured vertical profiles available for PFTBA, we calculate the GWP assuming constant, tropospheric, and stratospheric decay lifetime corrections.

There are no known lifetime measurements of PFTBA. Hong et al. [2] assumed a life time of 500 years and calculated a GWP of 7100, while 3M [3] claimed a lifetime of 2000 years leading to a GWP of 7200. Table 2 lists the GWP of PFTBA calculated for four different lifetimes and three VMR profile shapes averaged over temperature with the uncertainty reported as one standard deviation. We find that the GWP is most sensitive to lifetime, whereas the GWPs calculated with different VMRs agree with each other within one standard deviation. For the lifetimes of 500 and 2000 years, our results agree with the values of GWP previously reported in [2,3], respectively.

6. Conclusions

Temperature-dependent absorption cross-section measurements of PFTBA were made over the temperature range of 298–344 K. We find satisfactory agreement between our experimental cross-sections and theoretical DFT calculations. Our cross-section measurements also agree with previously published data [2]. Furthermore, no significant change in integrated band strength with temperature is observed and an average value of 7.81×10^{-16} cm/-molecule is obtained for the integrated band strength over the spectral range of 570–1400 cm^{-1}. Furthermore, the location of the centroid of each band also shows no significant change with temperature.

We calculate an average value over temperature of the instantaneous RE of PFTBA of 0.77 Wm^{-2} $ppbv^{-1}$, which agrees within error to previously published data [2]. We use these values to calculate the GWP for a range of lifetimes and assuming three different VMR profile regimes. The GWP of PFTBA ranges from 6874 to 7571, depending on choice of VMR shape and lifetime. Overall, we conclude that our measurements are consistent with

Table 2
GWP of PFTBA for different lifetimes and VMR profiles. GWPs are reported as the average of the GWPs calculated from the different REs in Fig. 7. Uncertainty is one standard deviation.

VMR profile	Lifetime (years)			
	500	1000	1500	2000
Constant	7035 ± 315	7387 ± 331	7509 ± 337	7571 ± 339
Exponential decay	6874 ± 308	7252 ± 325	7390 ± 331	7462 ± 334
Exponential growth	6996 ± 314	7355 ± 330	7481 ± 335	7546 ± 338
Hong et al. [2]	7100			
Costello et al. [3]				7200

the previously published data and that further attention be devoted to controlling PFTBA emissions into the atmosphere.

Acknowledgment

This work was supported by the Natural Sciences and Engineering Research Council of Canada (NSERC).

References

[1] P. Forster et al., Climate Change 2007: The Physical Science Basis, Cambridge Univ. Press, 2007. pp. 129–234.
[2] A.C. Hong, C.J. Young, M.D. Hurley, T.J. Wallington, S.A. Mabury, Geophys. Res. Lett. 40 (2013) 1–6.
[3] M.G. Costello, R.M. Flynn, J.G. Owens, 3M Company, John Wiley and Sons, Inc., 2014.
[4] T.J. Johnson, R.L. Sams, T.A. Blake, S.W. Sharpe, P.M. Chu, Appl. Opt. 41 (2002) 2831–2839.
[5] R.J. Bell, Introductory Fourier Transform Spectroscopy, Academic Press, 1972.
[6] K. Le Bris, L. Graham, J. Quant. Spectrosc. Radiat. Transfer 151 (2015) 13–17, http://dx.doi.org/10.1016/j.jqsrt.2014.09.005.
[7] K. Le Bris, K. Strong, S.M.L. Melo, J.C. Ng, J. Mol. Spectrosc. 243 (2007) 178–183.
[8] K. Le Bris, K. Strong, J. Quant. Spectrosc. Radiat. Transfer 111 (2010) 364–371.
[9] K. Le Bris, R. Pandharpurkar, K. Strong, J. Quant. Spectrosc. Radiat. Transfer 112 (2011) 1280–1285.
[10] K. Le Bris, J. McDowell, K. Strong, J. Quant. Spectrosc. Radiat. Transfer 113 (2012) 1913–1919.
[11] S.W. Sharpe, T.J. Johnson, R.L. Sams, P.M. Chu, G.C. Rhoderick, P.A. Johnson, Appl. Spectrosc. 58 (2004) 12.
[12] M.J. Frisch, G.W. Trucks, H.B. Schlegel, G.E. Scuseria, M.A. Robb, J.R. Cheeseman, J.A. Montgomery, Jr., T. Vreven, K.N. Kudin, J.C. Burant, J.M. Millam, S.S. Iyengar, J. Tomasi, V. Barone, B. Mennucci, M. Cossi, G. Scalmani, N. Rega, G.A. Petersson, H. Nakatsuji, M. Hada, M. Ehara, K. Toyota, R. Fukuda, J. Hasegawa, M. Ishida, T. Nakajima, Y. Honda, O. Kitao, H. Nakai, M. Klene, X. Li, J.E. Knox, H. P. Hratchian, J.B. Cross, V. Bakken, C. Adamo, J. Jaramillo, R. Gomperts, R.E. Stratmann, O. Yazyev, A.J. Austin, R. Cammi, C. Pomelli, J.W. Ochterski, P.Y. Ayala, K. Morokuma, G.A. Voth, P. Salvador, J.J. Dannenberg, V.G. Zakrzewski, S. Dapprich, A.D. Daniels, M.C. Strain, O. Farkas, D.K. Malick, A.D. Rabuck, K. Raghavachari, J.B. Foresman, J.V. Ortiz, Q. Cui, A.G. Baboul, S. Clifford, J. Cioslowski, B.B. Stefanov, G. Liu, A. Liashenko, P. Piskorz, I. Komaromi, R.L. Martin, D.J. Fox, T. Keith, M.A. Al-Laham, C.Y. Peng, A. Nanayakkara, M. Challacombe, P.M.W. Gill, B. Johnson, W. Chen, M.W. Wong, C. Gonzalez, J.A. Pople, Gaussian 03, Revision C.02, Gaussian, Inc., Wallingford CT, 2004.
[13] S. Pinnock, M.D. Hurley, K.P. Shine, T.J. Wallington, T.J. Smyth, J. Geophys. Res. 100 (D11) (1995) 23227–23238.
[14] O. Hodnebrog, M. Etminan, J.S. Fuglestvedt, G. Marston, G. Myhre, C.J. Nielsen, K.P. Shine, T.J. Wallington, Rev. Geophys. 51 (2013) 300–378.
[15] A.R. Ravishankara, S. Solomon, A.A. Turnipseed, R.F. Warren, Science 259 (1993) 194199.
[16] M.J. Prather, J. Hsu, Geophys. Res. Lett. 35 (2008) L12810, http://dx.doi.org/10.1029/2008GL034542.